Available online at www.sciencedirect.com
SCIENCE DIRECT®
Solar Energy Materials & Solar Cells
ELSEVIER
Solar Energy Materials & Solar Cells 86 (2005) 229–241
www.elsevier.com/locate/solmat

A photovoltaic cell incorporating a dye-sensitized ZnS/ZnO composite thin film and a hole-injecting PEDOT layer

Jung-Yu Liao, Kuo-Chuan Ho*

Department of Chemical Engineering and Institute of Polymer Science and Engineering, National Taiwan University, 1, Sec. 4, Roosevelt Road, Taipei 10617, Taiwan

Received 6 June 2004
Available online 11 September 2004

Abstract

A photovoltaic cell containing a dye-sensitized ZnS/ZnO composite thin film was studied. ZnS was thermally evaporated or electrodeposited onto conducting fluorine-doped tin oxide glass; then a particulate ZnO layer was pasted and sintered to form a ZnS/ZnO composite layer. A visible light source was utilized to excite the Ru-dye, which was adsorbed onto the surface of the ZnO. The ZnS layer is believed to provide an alternative pathway for electrons to move across ZnO barriers. This alternative pathway with the composite layer structure provides higher power efficiency than does a single layer of ZnO or ZnS. A hole-injecting, p-type poly(3,4-ethylenedioxythiophene) (PEDOT) thin film was also introduced to substitute for the Pt catalytic layer which helps with the rejuvenation of I^- ions. Although the p-type semiconductor behavior increased the open circuit voltage (V_{oc}), the power efficiency decreased because the I^- rejuvenation rate was much slower on PEDOT than on Pt.

Keywords: Electrodeposition; Photovoltaic cell; Poly(3,4-ethylenedioxythiophene) (PEDOT); Ru-dye; ZnO; ZnS

*Corresponding author. Tel.: +886-2-2366-0739; fax: +886-2-2362-3040.
E-mail address: kcho@ntu.edu.tw (K.-C. Ho).

0927-0248/$ - see front matter © 2004 Elsevier B.V. All rights reserved.
doi:10.1016/j.solmat.2004.07.006

1. Introduction

The electrochemical photovoltaic cell composed of dye-sensitized metal oxides has been widely investigated. First, as proposed by Grätzel et al., Ru-dye sensitized titanium dioxide (TiO_2) offers a respectably high power efficiency of around 10% [1] which raised the hope of fabricating a stable, highly efficient, electrochemical photovoltaic cell. Other metal oxides have also been tested, including SnO_2, ZnO, Nb_2O_5, Fe_2O_3, CdO, and MgO. Among them, ZnO has drawn much attention owing to its generally equal energy band level (3.0–3.2 eV) compared to TiO_2 in contrast to the others [2]. Hagfeldt et al. [3] reported a promising efficiency of 5% using ZnO nanoparticles, which exhibited the feasibility of being an alternative option for TiO_2. On the other hand, other semiconductors showing lower efficiency than TiO_2 have exhibited comparable values when used as composite films, such as SnO_2/MgO [4], CdS/MgO [5], ZnO/SnO_2 [6], and (Cd, Zn)S/(Cd, Zn)O [7]. It is interesting that a metal sulfide [5], which rarely adsorbs the Ru-dye is beneficial in raising the power efficiency. One of our objectives was to combine the advantages of high-efficiency ZnO films and the composite structure of ZnO/ZnS. Thus, a ZnS/ZnO composite thin film was fabricated in order to improve the performance of a cell based on the weakly dye-adsorbing ZnS.

ZnS, with a wide band gap of 3.6 eV, requires a UV light source to excite the photoactivity. Many methods have been used to fabricate ZnS thin films, including screen printing and sintering [7], electrochemical deposition [8,9], chemical bath deposition [10], thermal evaporation [11], MOCVD [11], sputtering [11], and MBE for doping processes [12]. In this work, both electrodeposition and thermal evaporation processes were used to fabricate films.

Poly(3,4-ethylenedioxythiophene), or PEDOT as shown in Fig. 1, is a polymer with a high p-conducting property in a conductivity range of 0.1–10 S/cm [13,14]. Many applications have been reported for this polymer, including electrochromic materials [15], sensors [16], antistatic coatings [17], and hole-injecting layers [18,19]. The hole-injecting layers, which are utilized as anodes have been widely used in LEDs [18] and p/n type photovoltaic cells [19]. Another objective of this work was to use PEDOT thin films to replace the common catalytic Pt layer (where I_3^- is reduced back to I^-), to see if we could improve the performance of the cell.

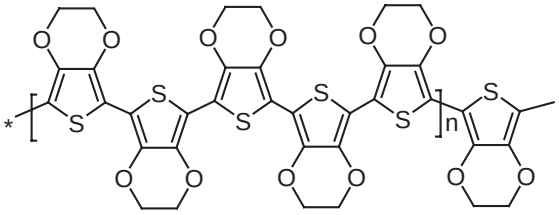

Fig. 1. Polymer structure of PEDOT.

2. Experimental

ZnS thin films were prepared by both electrodeposition and thermal evaporation methods. A cathodic potential of −0.7 V (vs. Ag/AgCl, sat'd KCl) was applied to the FTO glass ($R_{sh} = 50\,\Omega/\square$, Sinonar Corp., Hsinchu, Taiwan) immersed in an aqueous solution containing 0.1 M $ZnSO_4$ with or without 0.1 M HCl. The electrodeposition process was controlled at a charge density of $0.2\,C/cm^2$ with a potentiostat (PGSTAT30, Autolab Eco Chemie). The films that were electrodeposited in the solution without 0.1 M HCl were only used for UV-visible (UV-Vis) characterization. The other method for producing ZnS films was based on a thermal (vacuum) evaporation process. ZnS particles (97%, Showa) were heated at 3×10^{-5} Torr and condensed from the vapor phase onto the FTO glass. The film thickness was maintained at around 20 nm for fabricating the solar cell and at 1 μm for UV characterization. The instruments used for analysis of the prepared ZnS films were a UV-visible spectrometer (UV-1601PC, Shimadzu) and XRD ($\lambda = 1.5405$ Å, MO3XHF, Mac Science).

The ZnO coating was obtained by pasting ZnO particles suspended in a propylene carbonate (PC) solution with a trace amount of surfactant (Triton X-100, Sigma) and sintering them at 425 °C for 30 min. In the following discussion, a simplified symbol is used to identify each sample. A slash "/" denotes the interface of each layer, and the dye is usually denoted by the layer next to ZnO. The electrodeposited ZnS + ZnO is denoted by "ZnS + ZnO", while the thermally evaporated ZnS is simply denoted as "ZnS." A pure ZnO layer was obtained by pasting and sintering ZnO particles and is denoted by "ZnO". The composite film prepared in this study was obtained layer by layer, which differs from those of mixed layers reported in the literature [4–7]. The purpose of the layered structure was to increase the adsorptive surface area offered by the ZnO. The solution consisted of 0.2 g of ZnO powder in 5 ml PC with two drops of Triton X-100. The Ru-dye (bis(isothiocyanato)ruthenium (II)-bis-2,2′bipyridine 4,4′dicarboxylic acid, Ruthenium 535, Solaronix S.A., Aubonne, Switzerland) was adsorbed onto ZnO particles by immersing the ZnO-coated composite thin film into a dye containing ethanol solution.

The PEDOT thin film was electropolymerized onto the ITO glass ($R_{sh} = 25\,\Omega/\square$, Ritek, Hsinchu, Taiwan) with an active area of $1.5 \times 2\,cm^2$. The electropolymerization potential was set to 1.2 V (vs. Ag/Ag^+, 0.01 M $AgNO_3$ (= 0.47 V vs. NHE)), and the film thickness was controlled by the input charge density over the active area at a level of $50\,mC/cm^2$. The solution bath consisted of 0.01 M EDOT (3,4-ethylenedioxythiophen) monomer (Aldrich) and 0.1 M $LiClO_4$ in an acetonitrile solvent. The Pt thin catalytic layer was obtained by sputtering Pt onto the FTO glass. The electrolyte, which separates both electrodes with a 0.028-cm spacer (3 M tape), consisting of 0.5 M LiI + 0.05 M I_2 in acetonitrile, was used for making the cells. All materials were commercially available and were used as received without further purification.

The visible light illumination was tuned to simulate the sun light by an AM 1.5 solar simulator (model 81075, Oriel) in conjunction with IR and neutral density filters. The incident intensity was controlled at $20\,mW/cm^2$. The actual illuminated

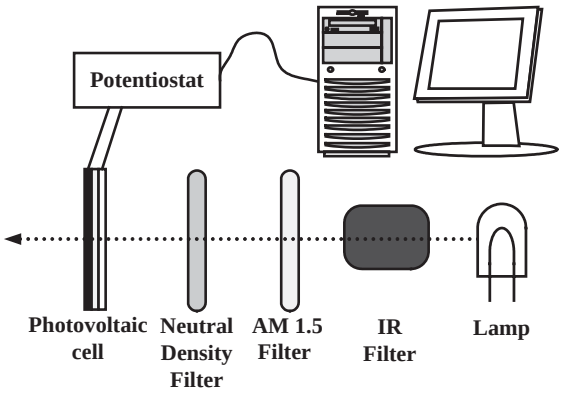

Fig. 2. Experimental setup for the visible illumination system as well as the in situ electrochemical data acquisition system.

area of the device was set to 1.2 cm^2. Photoelectrochemical data were obtained by the same potentiostat mentioned earlier. The entire illumination and data acquisition system is shown in Fig. 2.

3. Results and discussion

3.1. Electrodeposition of ZnS

It has been reported that ZnS can be electrodeposited by reducing $S_2O_3^{2-}$ anions to S^{2-} in an aqueous solution of $ZnSO_4$ and $Na_2S_2O_3$ [8,9]. The electrochemical reduction of $S_2O_3^{2-}$ can be obtained by rearranging the following electrochemical reactions with their standard reaction potentials (E^0):

$$SO_3^{2-} + 3H_2O + 6e^- \leftrightarrow S^{2-} + 6OH^-, E_1^0 = -0.61\,V\ (NHE), \quad (1)$$

$$2SO_3^{2-} + 3H_2O + 4e^- \leftrightarrow S_2O_3^{2-} + 6OH^-, \quad E_2^0 = -0.58\,V\ (NHE), \quad (2)$$

$$2H_2O + 2e^- \leftrightarrow H_2 + 2OH^-, \quad E_3^0 = -0.828\,V\ (NHE), \quad (3)$$

$$2H^+ + 2e^- \leftrightarrow H_2, \quad E_4^0 = 0\,V\ (NHE). \quad (4)$$

Thus, the overall reaction is obtained by combining Eqs. (1)–(4), or Eq. (1) × 2–Eq. (2)–Eq. (3) × 3 + Eq. (4) × 3, to obtain

$$S_2O_3^{2-} + 6H^+ + 8e^- \leftrightarrow 2S^{2-} + 3H_2O. \quad (5)$$

The E^0 of Eq. (5) is

$$E_5^0 = \frac{12 \times (E_1^0) - 4 \times (E_2^0) - 6 \times (E_3^0) + 6 \times (E_4^0)}{8} = -0.004\,V\ (NHE). \quad (6)$$

If the $S_2O_2^{2-}$ is also undergoing a reduction reaction, the electrochemical reduction of SO_4^{2-} to form SO_3^{2-} can be written as

$$SO_4^{2-} + H_2O + 2e^- \leftrightarrow SO_3^{2-} + 2OH^-, \quad E_7^0 = -0.90\,V\ (NHE) \tag{7}$$

and the overall reaction is obtained by combining Eq. (7) with Eqs. (1), (3), and (4) or Eq. (1) + Eq. (7)–Eq. (3) × 4 + Eq. (4) × 4, to give

$$SO_4^{2-} + 8H^+ + 8e^- \leftrightarrow S^{2-} + 4H_2O. \tag{8}$$

The E^0 of Eq. (8) is

$$E_8^0 = \frac{6 \times (E_1^0) + 2 \times (E_7^0) - 8 \times (E_3^0) + 8 \times (E_4^0)}{8} = 0.1455\,V\ (NHE). \tag{9}$$

The reduction of both $S_2O_3^{2-}$ and SO_4^{2-} can be driven by a potential of −0.7 V (vs. Ag/AgCl, sat'd KCl) in the present system, as judged by the calculated values of E_5^0 and E_8^0.

On the other hand, the electrodeposition of ZnO is also proposed based on the reduction of oxygen in an aqueous solution containing Zn^{2+} at a potential more negative than −0.7 V (vs. Ag/AgCl) [20–22]. The overall reaction proposed is [20]

$$Zn^{2+} + \frac{1}{2}O_2 + 2e^- \rightarrow ZnO, \quad E_{10}^0 = 0.93\,V\ (NHE); \tag{10}$$

however, the reduction of Zn^{2+} is described by

$$Zn^{2+} + 2e^- \rightarrow Zn, \quad E_{11}^0 = -0.76\,V\ (NHE). \tag{11}$$

The onset potential (−0.76 V (NHE) = −0.957 V (Ag/AgCl, sat'd KCl)) for Zn^{2+} reduction is more negative than the potential of −0.7 V (vs. Ag/AgCl, sat'd KCl) applied in this work. Therefore, the potential applied is sufficient to drive the deposition of both ZnS and ZnO according to the previous discussion while preventing the formation of metallic Zn.

The electrodeposited film is gray in appearance, which is caused by the presence of HCl. The difference in the prepared films, with or without HCl in the electrolyte during the electrodeposition process, is shown in Fig. 3(a). For the film electrodeposited in the presence of HCl, the absorption was approximately 6 times larger than that without HCl. To determine the band gap of these mixed ZnS + ZnO films, the spectra in Fig. 3(a) were replotted in Fig. 3(b), where $\alpha (= A\ln(10)/d$, with A as the absorbance and d the film thickness [23], which was estimated to be 1 μm) is the absorption (or attenuation) coefficient and E is the photo energy ($E = h\nu$). The band gap for the ZnO + ZnS film can be obtained by fitting data in Fig. 3(b) according to the following equation [24]:

$$\alpha E = k(E - E_g)^{1/2}, \tag{12}$$

where E_g is the band gap of a semiconductor, and k is a proportionality constant.

For films deposited without HCl, band gap values of around 3.6 and 3.0 eV were obtained, which correspond to ZnS and ZnO, respectively. The decreased band gap of ZnO was primarily due to the codeposition process that produces defects and

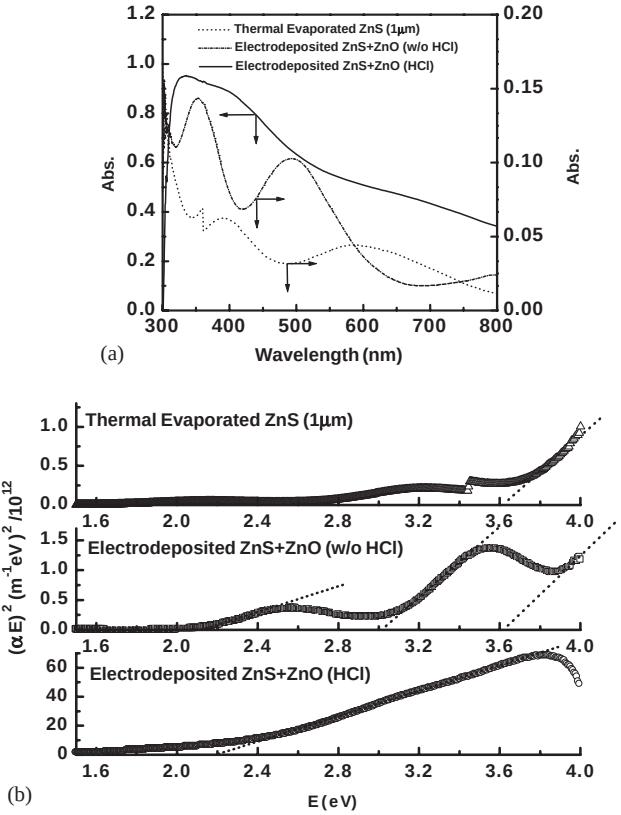

Fig. 3. (a) Full visible absorption spectrum for both the electrodeposited ZnS + ZnO with or without Cl^- and the thermally evaporated ZnS. (b) Band-gap determination from the UV spectrum.

tail-states [25], which are commonly seen in amorphous semiconductors. When HCl coexists in the solution bath, Cl^- doping significantly raises the overall spectrum which overwhelms (the intensity increases by about 6-fold) the absorbances of ZnS and ZnO (Fig. 3(a)). This makes it impossible to observe the band gap of a Cl^--doped, electrodeposited film (Fig. 3(b)).

A band gap with a value of 2.2 eV, rather than either of those for ZnS or ZnO, was obtained for Cl^--doped ZnS + ZnO. A similar band gap (2.1 eV) was also observed in an electrodeposited film without Cl^- doping. Since the band gap of tin oxide (SnO_2) is 3.8 eV, it is uncertain which species corresponds to this band gap of 2.1–2.2 eV. It is possible that a new species or a new structure was formed during the electrodeposition process, such as hydroxide formation ($Zn(OH)_2$, $Zn_5(OH)_8Cl_2$, etc. [20]). It is clear that these new species or new structure formation dominate during electrodeposition with Cl^- doping and cause absorption in the visible range.

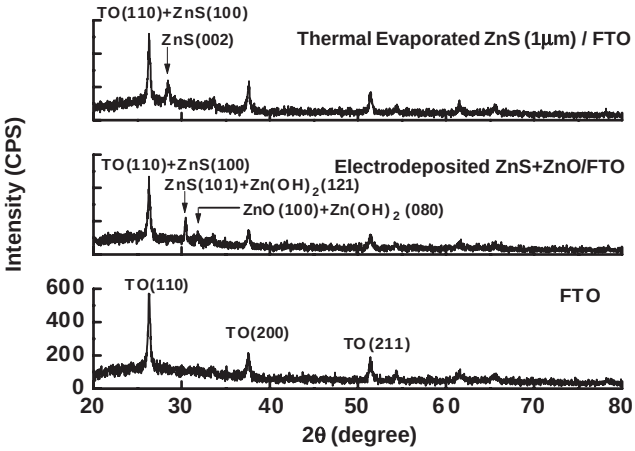

Fig. 4. XRD analysis of both the electrodeposited ZnS + ZnO (with HCl) and the thermally evaporated ZnS, compared with the background FTO.

The XRD analysis of the electrodeposited ZnS + ZnO thin film (with HCl) is shown in Fig. 4. It shows that ZnO (JCPDS#36-1451: $2\theta = 31.769$(1 0 0)), ZnS (JCPDS#36-1450: $2\theta = 26.914$ (1 0 0); 28.500 (0 0 2); 30.527 (1 0 1)) and $Zn(OH)_2$ (JCPDS#20-1437: $2\theta = 30.399$ (1 2 1); 31.104 (0 8 0)) are possibly codeposited on the FTO substrate (JCPDS#46-1088: $2\theta = 26.578$ (1 1 0); 37.768 (2 0 0); 51.755 (2 1 1)) and are coincident with the previous E^0 prediction, even though the band gaps of $Zn(OH)_2$ are unable to match the value (2.1–2.2 eV) obtained through UV-Vis techniques for films with and without Cl^- doping.

3.2. Thermal evaporation of ZnS

In this work, the ZnS film thickness prepared by thermal evaporation for photovoltaic cell is around 20 nm. However, this ultra-thin film is not easily detected by UV-Vis spectra. Thus, a much thicker film (1 μm) was deposited for characterization. The UV-Vis spectrum is shown in Fig. 3(a) together with that of the electrodeposited ones. For an electrodeposited film with Cl^- doping, the color is gray, and for a thermally evaporated one, it is almost transparent except in the UV range. The band gap of thermally evaporated ZnS is 3.6 eV, as seen from Fig. 3(b), thus only ZnS is deposited. The discontinuous jump at 3.4 eV is due to the instrumental mismatch when switching the light source from visible to UV. A slight perturbation is also noticeable for spectra of ZnS + ZnO samples prepared in the presence of HCl.

As for XRD, only the ZnS peak is shown in Fig. 4. This is reasonable because the powders are heated in a vacuum chamber (3×10^{-5} Torr); thus, the possibility of oxygen codeposition can be neglected, and only a ZnS film is obtained.

3.3. Efficiency

The configuration of the photovoltaic cell is shown in Fig. 5, with variation in the dye-sensitized layer in different cases. Because the Ru-dye molecules adsorb strongly onto the metal oxide [26], the presence of ZnS particles does not contribute to dye adsorption. The counter electrode is a thin, sputtered Pt layer onto the FTO glass and plays a role as a catalyst to facilitate the reduction of I_3^- ions and improve the rejuvenation efficiency of the dye.

The power efficiency is defined by the following equation [27]:

$$\eta_p = \frac{i_m V_m}{P_r} \times 100\%, \tag{13}$$

where $i_m V_m$ is the maximum multiplied value in the $i-E$ sweep (as in Fig. 6), and P_r is the illuminating power input, which is controlled to 20 mW/cm^2. The open circuit voltage (V_{oc}) is set at $i=0$, and short circuit current (I_{sc}) is defined at $V=0$.

Fig. 6 shows the $i-V$ characteristic of a dye-sensitized layer adsorbed on four different oxide layers. These data were obtained by the linear scanning voltage technique with a scan rate of 5 mV/s. Although there is a signal of ZnO codeposition in the electrodeposited film in the UV-Vis analyses (Fig. 3(b)) and XRD (Fig. 4), there was almost no adsorption of dye onto the film (for cell #1), as judged by the appearance. It is possible that the ZnO is located on the inner side of the layer, which was not exposed to the dye, and thus this may have been responsible for the low power efficiency of cell #1. This is because, theoretically, neither ZnS nor ZnO is primarily excited by visible light. The trace amount of dye adsorption leads to a low short-circuit current and a small power efficiency (η) of 0.08%. The V_{oc}, which is the

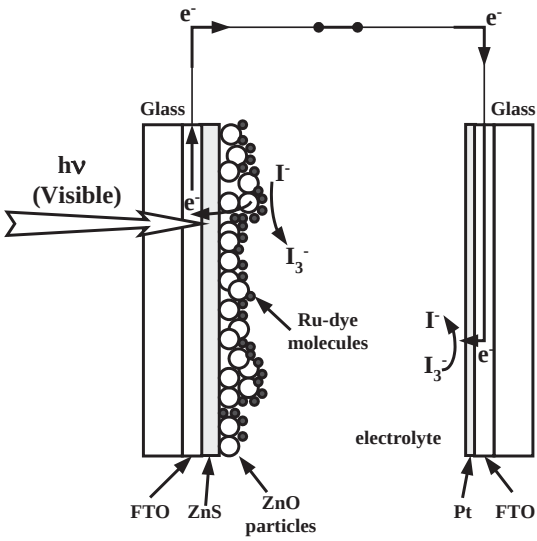

Fig. 5. General cell configuration of the dye-sensitized photovoltaic cell.

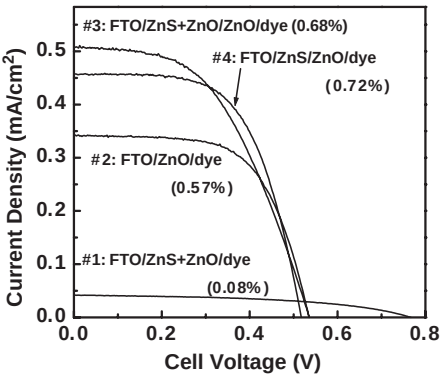

Fig. 6. *i–V* curve and power efficiency for various dye-sensitized solar cells with different thin-film preparations. The scan rate was 5 mV/s.

potential difference between the redox couple at the Pt electrode and the excited Fermi-level of the composite film (similar to Fig. 7(a) or Fig. 9), is high at up to 0.76 V.

The pure "ZnO/dye" (cell ♯2) was tested to have a power efficiency (η) of 0.57%, which is relatively low as compared to those ($\eta = 1.1$–5.0%) reported in the literature [3]. However, a lot of parameters will affect the overall performance, including particle size, porosity, surface area, the amount of dye adsorbed, the electrolyte type, the process for dye rejuvenation, etc. Compared to the highly efficient ZnO thin film preparation [3], it is understandable that the surface area was not sufficient in the present work because the film thus fabricated is close to particulate clusters rather than a film prepared with nanoparticles. That contributed to the insufficient surface area for dye adsorption as well as discontinuous electron transport through the huge ZnO cluster grains, which could have lowered the efficiency. On the other hand, reported films with compression resulted in more-efficient electron injection into ZnO [3], which explains the high performance.

The mechanism by which the dye functions and is rejuvenated is shown in Fig. 7(a). The excited dye (D^*) injects electrons into the conduction band of ZnO. Electrons are then transported through an outer circuit to the counter electrode, which reduces the I_3^- ions back to I^-. The dye is oxidized (D^+) after the electron injection. It is rejuvenated (D) by oxidizing I^- to I_3^-, and is then ready to be excited again [27].

The V_{oc} of cell ♯2 in Fig. 6 is 0.53 V, which is less than that of cell ♯1. Like the power efficiency, V_{oc} is also affected by many factors, including the type of semiconductor (Fermi-level), redox couple concentration, recombination of electrons and holes, the amount of dye, rejuvenation of the dye, etc. In this case, the decrease in V_{oc} was determined by the electron transfer resistance for the particulate ZnO layer, as opposed to the more-conductive "ZnS + ZnO" film in cell ♯1.

For the composite "ZnS + ZnO/ZnO/dye" film (in cell ♯3 with $\eta = 0.68\%$) or "ZnS/ZnO/dye" film (in cell ♯4 with $\eta = 0.72\%$) configuration shown in Fig. 6, the

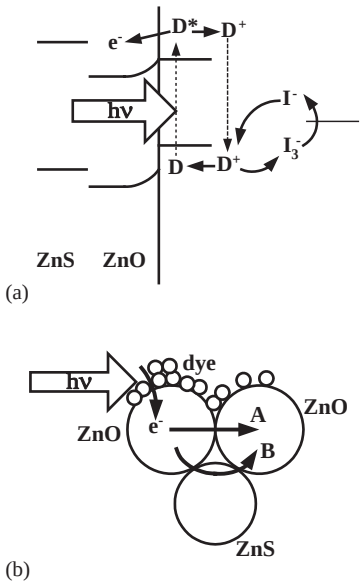

Fig. 7. (a) Relative energy diagram of a dye-sensitized photovoltaic cell with a ZnS/ZnO composite thin film. (b) Illustration of the ZnS fine layer that offers a faster alternative electron pathway "B" than the original pathway "A," which is full of barriers among ZnO particles.

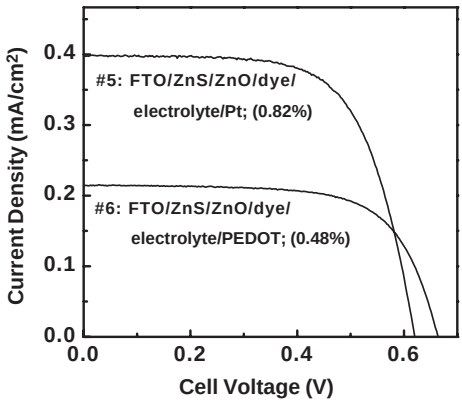

Fig. 8. *i–V* curve and power efficiency of cells made with Pt and PEDOT counter electrodes. The scan rate was 5 mV/s.

power efficiency is greater than that of the pure "ZnO/dye" configuration. But according to the relative band energy diagram (Fig. 7(a)), it is unlikely that the electrons are transported faster by penetrating the ZnS layer. The electrons seem to be trapped in the ZnO phase, because it is impossible for electrons to jump up to the conduction band gap of ZnS from ZnO. In fact, the same situation is also

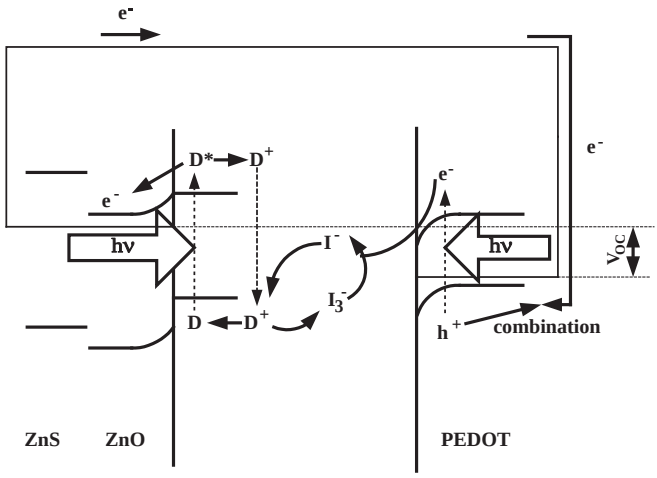

Fig. 9. Illustration of V_{oc} of a dye-sensitized photovoltaic cell with a ZnS/ZnO composite thin film and a hole-injecting, p-type PEDOT thin film.

encountered in other configurations [5,6]. One possible explanation is that electrons are injected into the ZnO when excited, and the rate-determining step of electron transport in the ZnO phase is overcoming the energy barrier of ZnO, as in pathway A illustrated in Fig. 7(b). As electrons continue to be injected into the ZnO or ZnO with much smaller particle sizes, the conduction band of ZnO shifts upwards, which makes it possible to transport electrons from ZnO to ZnS and back again [5,6], as in pathway B in Fig. 7(b). Because of the smaller contact area (larger barrier) compared with merely ZnO particles, the transport rate of pathway B offers a much-greater contact area or increases the necking between particles which lowers the electron charge transfer resistance and increases the power efficiency. Especially cell #4 in Fig. 6, with an ultra-thin layer of 20 nm of ZnS, offers more-seamless electron transport than that of pure ZnO (cell #2). A similar electron transfer-accelerating mechanism is also seen in the post treatment of $TiCl_4$ in TiO_2-based dye-sensitized solar cells, which facilitates the percolation of electrons from one particle to another [1].

3.4. The hole-injecting layer, PEDOT

A hole-injecting PEDOT was used to substitute for the Pt layer in Fig. 5. It was assumed that PEDOT also possesses p-type semiconductor characteristics since PEDOT is a highly hole-conducting (p-conducting) polymer with a band gap of 1.6 eV when kept in the doping state [14]. The performance for composite "ZnS/ZnO" cells with Pt or with PEDOT as the counter electrode is shown in Fig. 8. The configuration of cell #5 is identical to that of cell #4 in Fig. 6. It can be seen that the cell efficiency with PEDOT as the counter electrode is less than that of Pt, but the V_{oc} is higher. It is supposed that PEDOT possesses the p-type semiconductor property due to its high p-conductivity, as shown by the relative energy diagram in Fig. 9.

Like the dye, PEDOT is also excited when illuminated. The separation of holes and electrons from the PEDOT side helps to reduce the redox couple. The holes, which are left, are transported through the PEDOT and combine with the electrons that are transported from the outer circuit. It is the p-type PEDOT that contributes to the higher V_{oc}; however, PEDOT has a poor ability to catalyze the reduction of the redox couple even though it is a good hole conductor. The poor catalyzing ability contributes to the generation of fewer I^- ions, which hinders dye rejuvenation at the other side and lowers the power efficiency. Another possible reason for the lower efficiency may be the anionic (ClO_4^-) doping of the p-conducting PEDOT. It is likely that an anionic redox couple (I^-/I_3^-) is also inserted into PEDOT, which lowers the concentration of the redox couple in the electrolyte. It should be noted that the diagram shown in Fig. 9 is the ideal case for V_{oc}, which is defined under no outer current flows. When an electric current is passed, it is likely that PEDOT is reduced to an undoped state, so that it is no longer a p-conducting polymer any more [13,14], if the I^--catalyzing rate (or the hole-producing rate) in PEDOT is slower than that of the electron injection rate from the Ru-dye. All cell configurations as well as their performances are outlined in Table 1.

4. Conclusions

This work reports on the possibility of improving the power efficiency by demonstrating the feasibility of developing a composite ZnS/ZnO approach. The addition of ZnS might contribute a second route for electrons when they are being transported through the ZnO barriers. Electron transport is possible from ZnO to ZnS for smaller ZnO particles or continuing electron injection, which raises the Fermi-level. The maximum power efficiency of a composite ZnS/ZnO photovoltaic cell of 0.82% is thus obtained. Even though both ZnS and ZnO are electrodeposited, the limited and buried ZnO, however, does not provide sufficient surface area for adsorption of the dye. PEDOT was tested to show that the p-type characteristic as the V_{oc} of the cell increases. However, PEDOT is not a good catalyst for reducing the redox couple, which is regarded as necessary for efficient dye rejuvenation.

Table 1
List of proposed cell configurations with their performances

Cell no.	Configuration	V_{oc} (V)	I_{sc} (mA/cm^2)	η (%)	F.F. (%)
1	FTO/ZnS + ZnO/dye/electrolyte/Pt/FTO	0.76	0.042	0.08	0.59
2	FTO/ZnO/dye/electrolyte/Pt/FTO	0.53	0.34	0.57	0.76
3	FTO/ZnS + ZnO/ZnO/dye/electrolyte/Pt/FTO	0.53	0.51	0.68	0.60
4	FTO/ZnS/ZnO/dye/electrolyte/Pt/FTO	0.51	0.46	0.72	0.73
5	FTO/ZnS/ZnO/dye/electrolyte/Pt/FTO	0.62	0.40	0.82	0.79
6	FTO/ZnS/ZnO/dye/electrolyte/PEDOT/FTO	0.66	0.22	0.48	0.79

Acknowledgements

This work was sponsored by the National Research Council of the Republic of China under Grant number NSC 92-2623-7-002-005-NU.

References

[1] C.J. Barbé, F. Arendse, P. Comte, M. Jirousek, F. Lenzmann, V. Shklover, M. Grätzel, J. Am. Ceram. Soc. 80 (1997) 3157.
[2] K. Keis, J. Lindgren, S.-E. Lindquist, A. Hagfeldt, Langmuir 16 (2000) 4688.
[3] K. Keis, E. Magnusson, H. Lindström, S.-E. Lindquist, A. Hagfeldt, Sol. Energy Mater. Sol. Cells 73 (2002) 51.
[4] K. Tennakone, J. Bandara, P.K.M. Bandaranayake, G.R.A. Kumara, A. Konno, Jpn. J. Appl. Phys. 40 (2001) L732.
[5] P.K.M. Bandaranayake, P.V.V. Jayaweera, K. Tennakone, Sol. Energy Mater. Sol. Cells 76 (2003) 57.
[6] (a) K. Tennakone, I.R.M. Kottegoda, L.A.A. De Silva, V.P.S. Perera, Semicond. Sci. Technol. 14 (1999) 975;
(b) K. Tennakone, G.K.R. Senadeera, V.P.S. Perera, I.R.M. Kottegoda, L.A.A. De Silva, Chem. Mater. 11 (1999) 2474.
[7] A. Olea, P.J. Sebastian, Sol. Energy Mater. Sol. Cells 55 (1998) 149.
[8] C.D. Lokhande, M.S. Jadhav, S.H. Pawar, J. Electrochem. Soc. 136 (1989) 2756.
[9] C.D. Lokhande, V.S. Yermune, S.H. Pawar, J. Electrochem. Soc. 138 (1991) 624.
[10] T. Yamaguchi, Y. Yamamoto, T. Tanaka, Y. Demizu, A. Yoshida, Thin Solid Films 281–282 (1996) 375.
[11] T. Orent, J. Electrochem. Soc. 141 (1994) 1320.
[12] T. Yasuda, B.-P. Zhang, Y. Segawa, J. Crystal Growth 175/176 (1997) 583.
[13] H.J. Ahonen, J. Lukkari, J. Kankare, Macromolecules 33 (2000) 6787.
[14] L.B. Groenendaal, F. Jonas, D. Freitag, H. Pielartzik, J.R. Reynolds, Adv. Mater. 12 (2000) 481.
[15] M.-A. De Paoli, G. Casalbore-Miceli, E.M. Girotto, W.A. Gazotti, Electrochim. Acta 44 (1999) 2983.
[16] D. Setiadi, Z. He, J. Hajto, T.D. Binnie, Infrared Phys. Technol. 40 (1999) 267.
[17] F. Jonas, G.-D. Wolf, US Patent 05403467 (1995).
[18] M. Granström, M. Berggren, O. Inganäs, Science 267 (1995) 1479.
[19] A. Dhanabalan, J.K.J. van Duren, P.A. van Hal, J.L.J. van Dongen, R.A.J. Janssen, Adv. Funct. Mater. 11 (2001) 255.
[20] S. Peulon, D. Lincot, J. Electrochem. Soc. 145 (1998) 864.
[21] T. Yoshida, M. Tochimoto, D. Schlettwein, D. Wöhrle, T. Sugiura, H. Minoura, Chem. Mater. 11 (1999) 2657.
[22] M. Izaki, T. Omi, Appl. Phys. Lett. 68 (1996) 2439.
[23] I. Kosacki, V. Petrovsky, H.U. Anderson, Appl. Phys. Lett. 74 (1999) 341.
[24] Y. Wang, A. Suna, W. Mahler, R. Kasowski, J. Chem. Phys. 87 (1987) 7315.
[25] K. Morigaki, Physics of Amorphous Semiconductors, Imperial College Press, Singapore, 1999, p. 331.
[26] K. Westermark, H. Rensmo, A.C. Lees, J.G. Vos, H. Siegbahn, J. Phys. Chem. B 106 (2002) 10108.
[27] A.J. Bard, Integrated Chemical Systems, Wiley, New York, 1994, p. 267.